

Training-Free Style and Content Transfer by Leveraging U-Net Skip Connections in Stable Diffusion 2.*

Ludovica Schaerf
Max Planck Society
University of Zurich
Zurich, Switzerland

ludovica.schaerf@uzh.ch

Andrea Alfarano
Max Planck Society
University of Zurich
Zurich, Switzerland

andrea.alfarano@uzh.ch

Fabrizio Silvestri
Sapienza University of Rome
Rome, Italy

fsilvestri@diag.uniroma1.it

Leonardo Impett
University of Cambridge
Cambridge, United Kingdom

li222@cam.ac.uk

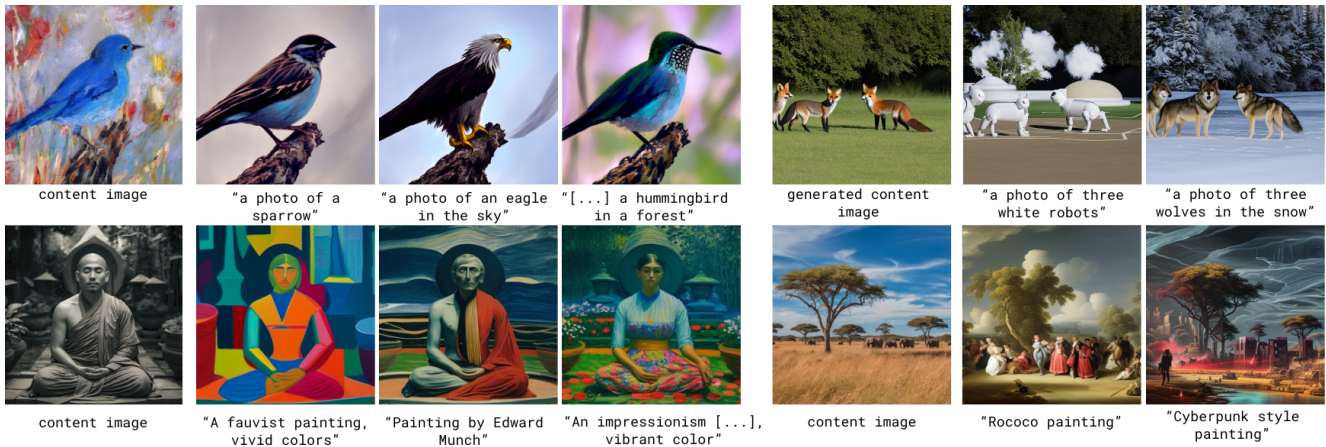


Figure 1. SkipInject: our method uses the $l=4$ and $l=5$ skip connections of Stable Diffusion 2.* to obtain flexible content and style transformations. From a painted “content image” of a bird, the model smoothly modifies the subject to resemble various species (e.g., sparrow, eagle) while retaining the overall scene. A generated image of foxes is transformed into “three white robots” and “three wolves in the snow,” with coherent and realistic alterations. Furthermore, the styles of the two content images are altered holistically, in aesthetics, subjects, and settings.

Abstract

Despite significant recent advances in image generation with diffusion models, their internal latent representations remain poorly understood. Existing works focus on the bottleneck layer (h -space) of Stable Diffusion’s U-Net or leverage the cross-attention, self-attention, or decoding layers. Our model, SkipInject takes advantage of U-Net’s skip connections. We conduct thorough analyses on the role of the skip connections and find that the residual connections passed by the third encoder block carry most of the spatial information of the reconstructed image, splitting the content

from the style. We show that injecting the representations from this block can be used for text-based editing, precise modifications, and style transfer. We compare our methods state-of-the-art style transfer and image editing methods and demonstrate that our method obtains the best content alignment and optimal structural preservation tradeoff.

1. Introduction

Recent advances in diffusion models have demonstrated surprising possibilities for image and video generation. Pioneered by models like Stable Diffusion [37], Midjourney,

and Dall-E [35], the generated artifacts are radically changing both online amateur communities and the creative industries (e.g., professional illustration).

Despite the success of image generation, these models’ internal representations are still poorly understood, limiting our ability to control or edit the resulting images effectively. In fact, precise and controlled generation is still an open question in Text-to-Image (TTI) models, often reliant on case-to-case fine-tuning or allowing limited control.

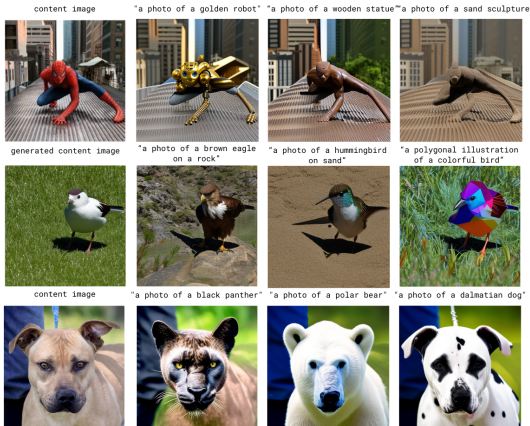


Figure 2. Examples of image editing results on Wild-TI2I and ImageNet-R-TI2I real and generated images.

Previous generations of image generation models, including Variational Autoencoders [23] and Generative Adversarial Networks [21], leverage the latent space of the bottleneck layer to determine editing directions [15, 21, 42]. Diffusion models [17, 43] are based on a Markov chain denoising process and inherently lack a single latent space. Furthermore, the noise prediction backbone is either a Diffusion Transformer (DiT) [31] or a U-Net [38], both architectures lacking a clear choice of latent space. In the context of U-Net backbones - the focus of this paper -, training-free approaches to image editing focus on swapping different modules of the denoising architecture, including the self- and cross-attention modules and the h-space, the bottleneck of the U-Net. However, an essential element within the U-Net, aiding the transmission of long-range dependencies and the gradient propagation, is the skip connection. In contrast to existing work, we focus on the former and its role in U-Net-based diffusion models.

In the remainder of the paper, we address the following questions: (i) How and where is information represented in the skip connections of the U-Net? (ii) How does it influence the image generation? (iii) When does this information arise during the denoising process?¹

In the first part of the paper, we address the previous

¹We also address (iv) Is the phenomenon consistent across different versions of Stable Diffusion? in the Supplementary Materials.

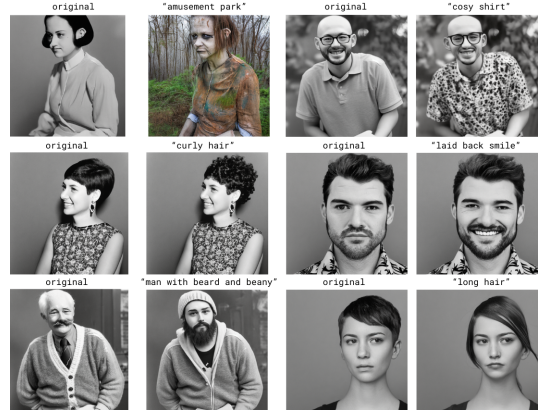


Figure 3. Image editing results on generated faces. We show precise transformations ranging from subtle changes, like makeup and hairstyle adjustments, to more global effects, including zombie-like effects. Our model preserves the core identity of each subject, maintaining facial structure.

questions in Sec. 4. In the second, we propose a training-free, controllable method that leverages the findings of the previous section to manipulate generated images. Namely, we find that injecting the second and third skip connections of the second group of connections from image *A* to image *B* transfers the spatial configuration of image *A* onto image *B*. Conversely, we find that image *B* transfers the style to image *A* when changing the second skip connection of the second group, naturally performing style transfer. Additionally, leveraging the injection timestep controls the appearance of the background of image *B* over image *A*, and modulating the mixing on the embedding offers control of the strength of the injection.

We demonstrate that an informed use of the properties of Stable Diffusion can achieve state-of-the-art performance on a wide variety of tasks, offering ample control over the intensity and nature of the output. In Sec. 5, we highlight the superiority of our method in achieving text-based image editing and style transfer and show preliminary results on fine-grained feature editing in Fig. 3.

To summarize, we contribute as follows:

- We investigate the role of the skip connections in the U-Net of Stable Diffusion, assessing their properties, their influence on the image, and variation across time steps.
- We propose an efficient and controllable image editing method and prove superiority or on-par SOTA performance on transferring content and style.
- Lastly, we propose three alternatives to modulate the editing effect.

2. Related work

In this section, we shortly explain the importance of latent space studies in the contexts of media studies and digital

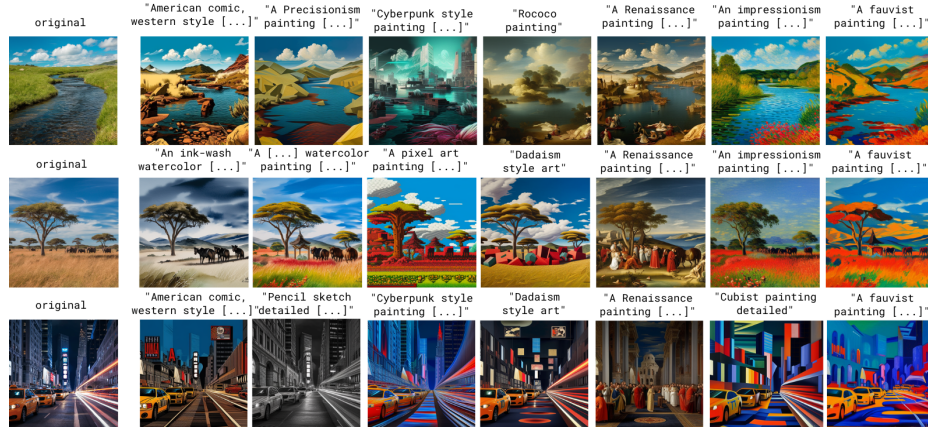


Figure 4. Examples of style transfer results on the Artist dataset [20].

arts to further motivate the focus of this paper. Successively, we cover image editing methods on Stable Diffusion.

2.1. Latent space in the arts and humanities

The latent space, understood strictly as the space where the data lies in the bottleneck layer of a model, is a topical entity for studying and understanding models beyond technical fields. These spaces are studied as n -dimensional cultural objects [36]. The latent spaces make continuous and spatialized the cultural knowledge fed into or generated by the model, creating an implicit meaningful organization [41]. These representations can be then studied as a map of culture [48], and can, in turn, be used to study models as cultural snapshots of reality [8, 18, 49, 50].

Digital artists and creative industries extensively used latent space-rooted methodologies, such as latent space walks and interpolation, to take advantage of the semantic continuity of this space. Initiating with DeepDream [2], the latent space continuity, opposed to reality’s fragmentation, creates an attractive space of artistic hallucination [1].

2.2. Image manipulation

In this section, we present some of the pivotal works in this direction, organized by what element is used for editing.

Latent code-based editing. Asyryp [24] uses the h -space and CLIP supervision to find a direction of modification in the space at each timestep, to add to the original latent in the denoising process through a modified Diffusion Deterministic Implicit Model (DDIM) [44]. Boundary diffusion [53], on the other side, computes a modification direction that is injected only at the mixing step, testing both ϵ -space and h -space. Haas *et al.* [12], among other findings, show that injecting the h -space of an image into another image changes the high-level semantics while retaining the structure and background. InjectFusion [19] observe the same phenomenon, implementing a calibrated procedure to inject the new h -space, maintaining the same correlation

to the skip connections. These methods are mostly based on unconditional DDPM-based models trained on specific datasets for *e.g.* CelebA.

Module-based editing. Prompt2Prompt (P2P) [14] substitute the cross-attentions of the U-Net layers to obtain text-based image editing. Plug and Play (PnP) [47] find that accurate editing can be achieved by injecting the spatial features of the middle decoding and self-attention layers. Closely related to the two previous works, Liu *et al.* [25] investigate the role of the cross-attention and the self-attention in the different feature layers, observing again that intermediate features are the most salient. Finally, Artist [20] shows that using the middle residual blocks as PnP to control the content and the cross-attentions to inform the style obtains successful text-driven stylization.

Text-based editing. A common alternative for diffusion models leverages the manipulation of text conditioning. Methods like DiffusionCLIP [22] and InstructPix2Pix [5] fine-tune the model or the text conditioning to obtain desired edits. Various successful methods tackle personalizing the outputs to specific entities such as Dreambooth [39]. Lastly, methods like SDEdit [9] leverage partial inversion and text-guided generation to achieve fast, training-free editing.

Adapters. Other popular methods leverage adapters, including ControlNet [51] and T2IAdapter [28] to increase the modalities that can be used to control the diffusion process. In fact, they train an ad-hoc adapter for each additional modality, obtaining perceptually interesting outcomes. To increase the manipulability, other methods make use of specifically trained LoRA adapters, like PreciseControl [29] CTRLorALter [45], LoRAadapter [11], which can achieve controlled modifications for the trained semantic.

2.3. Novelty

Disentanglement-based and adapters-based methods require learning each semantic or modality separately, hindering their generalization. Text-based methods either require ad-hoc fine-tuning or achieve partial control. Among the methods focusing on module-based editing, none demonstrates the generalization of the technique to both style transfer and text-based content editing. Compared to these methods, our approach is the simplest but allows the greatest control, using numerous plug-ins to mitigate the effect. Lastly, we tested that our method performs well on Turbo alternatives, obtaining the fastest results².

3. Preliminaries

In this section, we briefly recall the definition of Latent Diffusion Models (LDMs) by Rombach *et al.* [37], focusing on the architecture of the U-Net [38] backbone.

3.1. Latent Diffusion

Latent Diffusion Models (LDMs) address the computational and memory limitations of diffusion models by performing the diffusion process in a compressed latent space rather than the high-dimensional image space. Specifically, LDMs utilize a pre-trained autoencoder to encode images x_0 into a lower-dimensional latent representation $z_0 = E(x_0)$, where E denotes the encoder. The diffusion process is then applied to z_0 instead of x_0 , significantly reducing the computational resources required for training and sampling.

The forward diffusion process in the latent space is defined as:

$$z_t = \sqrt{\alpha_t} \cdot z_0 + \sqrt{1 - \alpha_t} \cdot \epsilon, \quad (1)$$

where $\epsilon \sim N(0, I)$ is Gaussian noise, and $\{\alpha_t\}$ represents a predefined noise schedule. The model learns to predict the added noise ϵ using a neural network $\epsilon_\theta(z_t, t)$ during training. The training objective minimizes the expected loss:

$$\mathcal{L}(\theta) = \mathbb{E}_{z_0, \epsilon, t} \left[|\epsilon - \epsilon_\theta(z_t, t)|^2 \right], \quad (2)$$

where t is uniformly sampled from the diffusion steps.

3.2. Components of the U-Net

In this work, we exploit a pre-trained text-conditioned Latent Diffusion Model (LDM) with U-Net backbone, commonly known as Stable Diffusion (versions 1.4, 1.5, 2, 2.1, XL).

In Stable Diffusion, the traditional U-Net [38] is augmented with attention modules—residual blocks, self-attention blocks, and cross-attention blocks—with cross-attention enabling text conditioning.

²Results on Turbo can be found in Appendix.

In particular, the **residual block** processes the latent features ϕ_t^{l-1} from the previous layer $l - 1$ to produce intermediate features f_t^l and the latent features inputted to the following block ϕ_t^l :

$$f_t^l, \phi_t^l = \text{ResBlock}(\phi_t^{l-1}), \quad (3)$$

where ResBlock includes convolutional operations and activation functions that capture local patterns in the data.

4. Analysis

As explained in the previous section, skip connections are a critical component of the U-Net backbone, allowing long-range information flow and avoiding the vanishing gradient problem. However, their role within the Stable Diffusion models remains unknown. In this section, we present our investigation of the role of each skip connection, the time steps, and the properties of these embeddings to shed some light on these behaviors.

4.1. The role of skip connections

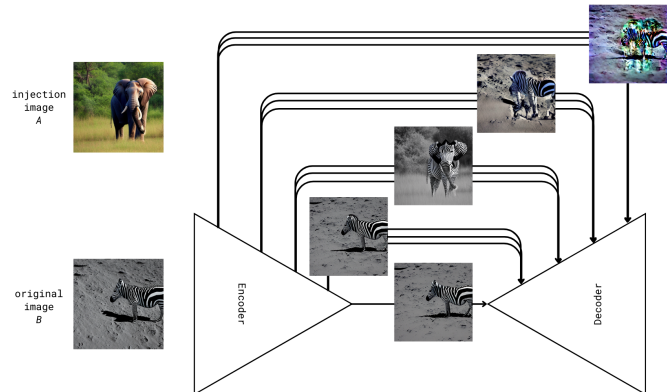


Figure 5. Visualization of the effect of switching each group of skip connections. We show the result of each skip connection switched on the respective swapped group. We observe that the h -space has an almost imperceptible effect on the final image, contrary to research into the disentanglement of DDPMs. The first group of skip connections closest to the h -space similarly has a limited effect, whereas the most coherent blending occurs in the second group of skip connections. The third group has no coherent effect on the image, generating random distortions, while the fourth performs akin to raw pixel blending.

In Stable Diffusion, the U-Net consists of four downsampling blocks (downblocks) and corresponding upsampling blocks connected via skip connections. Each downblock layer passes three residual connections alongside the main output. The skip connections consist of four sets of three residuals within the latent space (h -space).

To analyze the effect of each skip connection, we store the skip connections of an injection image A and test the

injection of each skip connection and combinations of them into the original image B . We start from a common initial noise z_t . We follow two different noise selection strategies: (i) we randomly sample a z_t from a Gaussian distribution, or (ii) we use the result of the DDIM inversion of either A , i.e., z_t^A , or B , i.e., z_t^B . We first fully denoise z_t with the prompt of image A , p^A , and store the skip connection f_t^l at each time-step t . Successively, we denoise z_t using the prompt of image B , p^B . At each time-step from t_{start} to t_{end} , we substitute the skip connection f_t^l of image A . We show an example of the effect we obtain by substituting each group of three skip connections (group 1: $l = 1, 2, 3$; group 2: $l = 4, 5, 6$; group 3: $l = 7, 8, 9$; group 4: $l = 10, 11, 12$) and the h -space in Fig. 5.

Previous studies [20, 25, 47] indicate that the middle decoding layers or the middle cross- and self-attention blocks are the most determinant of the content, suggesting that the structural information is formed roughly halfway in the decoding blocks. While our method aligns with previous findings, being the second group of skip connections roughly halfway in the depth of the model, it suggests that this information is already encoded in the encoder and passed through the decoder via the residual block.

Accepting standard distinctions of foreground-background and content-style³, we observe that the injection of the second group of skip connections of image A into image B preserves the background style of image B , in this case, the color scheme, the foreground style of image B , the stripes of the zebra, the background content of image A , the Savannah, and the foreground content of image A , the silhouette of the elephant.

4.2. The effect of the timesteps

In this section, we investigate the role of timesteps in the diffusion process (see Fig. 7) by injecting the skip connection of image A into image B at $t_{start} \neq 1000$ and $t_{end} \neq 0$. We observe that the first 150 steps ($t_{start} = 850$) have little impact on the final image, while the last 150 steps ($t_{end} = 150$) only serve as refinement, as found also in Asyrp [24]. We find that the skip connection of image A or image B for the first 500 denoising steps determines the content of the foreground, while the last 500 steps determine the background.

4.3. Modulating the effect

To achieve more controllable results, we investigate methods to modulate the intensity of the change.

Injection classifier-free guidance. Inspired by classifier-free guidance [16], we test the use of a linear combination of the injected embedding and original embedding

³While these terms do not have a precise definition, by content, we generally mean the structure of the object, and by style, the colors, textures, and patterns.

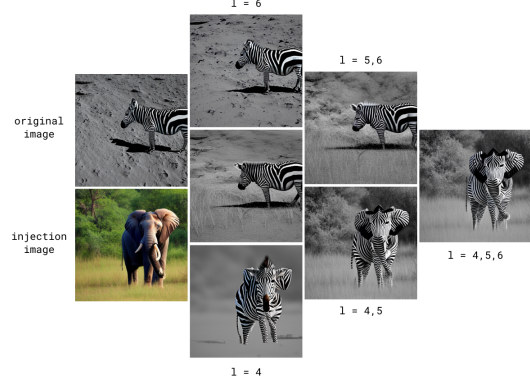


Figure 6. Close up into the second group of skip connections. The image shows the effect of this group’s different combinations of connections. From the bottom to the top, we injected only one of the skip connections, groups of two, and finally, all three. Specifically, we observe that the combination of $l = 4$ and $l = 5$ carry the most information: $l = 5$ injected alone creates a minimal change in the image but, when combined with $l = 4$, determines the spatial structure of the output. $l = 4$ alone conveys structure only of the foreground.

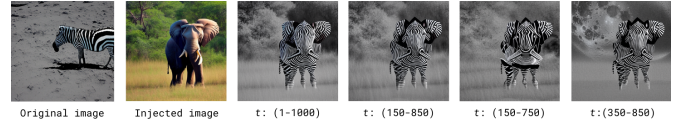


Figure 7. Visualization of the effect of the injection timesteps. We observe that starting the injection later at $t_{start} < 850$ leads to distortions in the foreground content while ending the denoising earlier at $t_{end} > 150$ reveals the background content of the original image. This phenomenon is consistent for every image we generate.

of the changed skip connections, parametrized by γ to balance the intensity of the mix. At each denoising step, the injected embedding becomes:

$$f^A(t, l) = f^B(t, l) + \gamma(f^A(t, l) - f^B(t, l)) \quad (4)$$

where t is the denoising timestep and l the skip connection layer.

Depth-wise alternation of the spatial embedding of the skip connections. The h -space and each skip connection are high-dimensional matrices with depth, width, and height channels. For instance, the layer $l = 4$ for a 512×512 output size is $1280 \times 16 \times 16$, so $depth = 1280$ and $width = height = 16$, as opposed to traditional latent spaces of GANs and VAEs of size 512. We hypothesize that the information stored in these embeddings is, therefore, highly redundant and attempt to investigate the nature of these spaces’ spatial features (width and height). We plot these embeddings as 1280 images of 16×16 pixels and we find that over 90% of the kernels show the same shape

with varying average or inverse intensities. Therefore, we suspect redundancy in the depth channel.



Figure 8. Visualization of modulation methods. We show the effects of the two modulation methods at $\gamma = r \in [0, 1]$. We observe that both methods achieve a successful modulation of the intensity of the effect and empirically observe that the use of both methods together obtains the best results. The advantage of the guidance is that it can surpass the effect above 1, but, differently from the second modulation method, it struggles in areas around 1, where the image should be similar to the non-modulated effect.

We leverage this observation to introduce an additional modulation method: we alternate at a ratio r the kernels of $f^A(t, l)$ with those of $f^B(t, l)$. That is to say, for every $1280 \times r \times 16 \times 16$ kernels, we inject the injection kernel and maintain the original one in the other cases.

In sum, the injection timing can control whether the background is retained or replaced with that of the original image, and the injection strength can be further modulated using classifier-free guidance and depth-channel alternation.

5. Experiments

We evaluate our method on **image editing** and **style transfer**, providing both quantitative metrics and qualitative results.

5.1. Experimental Setup

To evaluate our method on text-guided image-to-image and text-to-image translation, we follow established benchmarks, utilizing the Wild-TI2I dataset [47] and ImageNet-R-TI2I [47]. We adopt the protocol outlined in [20] for style transfer evaluation to text-guided style transfer.

Our evaluation employs two complementary metrics. First, text-image CLIP similarity quantifies how closely the generated images align with the style or edit prompts [34]. Second, the distance between DINO ViT self-similarity [7] assesses the degree of structure preservation. Additionally, we use LPIPS [52] to measure perceptual similarity, where lower values indicate better content retention.

We implement our method with the `Diffusers` library, using a custom `2DUNetConditional` model based on pre-trained weights from `stabilityai/stable-diffusion-2-base`. For image-to-image translation, we apply the `DDIMInverseScheduler` with 50 steps, generating images with the `UniPCMultistepScheduler`

using 50 inference steps and a guidance scale of 7.5.

5.2. Image editing

Qualitative Analysis provides a comparative analysis with previous methods. Competing methods frequently exhibit issues: Free Prompt Editing lacks style specificity (e.g., "penguin embroidery" fails to capture the embroidery texture), Prompt2Prompt does not follow the prompt effectively (the horse is not in the museum), and Plug-and-Play leads to feature distortions (e.g., "silver robot"). SDEdit struggles with structural integrity at high noise levels, while DiffEdit and MaCaCntrl lose context (e.g., the "teddy bear" is distorted). In contrast, our model consistently delivers prompt-specific transformations with high structural fidelity, demonstrating robustness across various styles and editing demands.

Quantitative analysis Quantitatively, we present the performance of our methods on the ImageNet-R-TI2I and Wild benchmarks. In Fig 10 we evaluate our model with CLIP cosine similarity (indicating prompt fidelity) and DINO-ViT self-similarity (indicating structural preservation). Across all benchmarks (Wild-TI2I, ImageNet-R-TI2I, and Generated ImageNet-R-TI2I), our model consistently balances high CLIP similarity with low DINO self-similarity, outperforming other methods like SDEdit, VQGAN-CLIP, and DiffuseIT in both text alignment and structural accuracy. Notably, our approach consistently places in the "Better" region, reflecting superior text fidelity and structural integrity.

5.3. Style Transfer

Qualitative evaluation Figure 11 offers a comparative analysis, highlighting distinctive performance variations among competing models. Models like DiffStyler, CLIPStyler, and Plug-and-Play often compromise the fidelity of the original content structure, leading to blurred or distorted shapes, particularly in intricate or highly abstract styles. NTI+P2P exhibits minimal style alteration, evident in the "8-bit pixel art" transformation, where the ship closely resembles the original. However, it is relevant to note that while these models demonstrate varying degrees of style application, evaluating artistic styles can be inherently arbitrary. Styles intended as artistic movements are sometimes conflated with specific methods, making objective assessment challenging. For instance, applying a "Dadaism style" prompt may focus on collage techniques rather than capturing the movement's conceptual essence.

In contrast, our model achieves a balanced and coherent output across styles, effectively preserving not only the content structure and the stylistic features but also adjusting the people, clothing, and objects in a historically coherent manner (as in Fig. 11). For example, in the "Impressionist

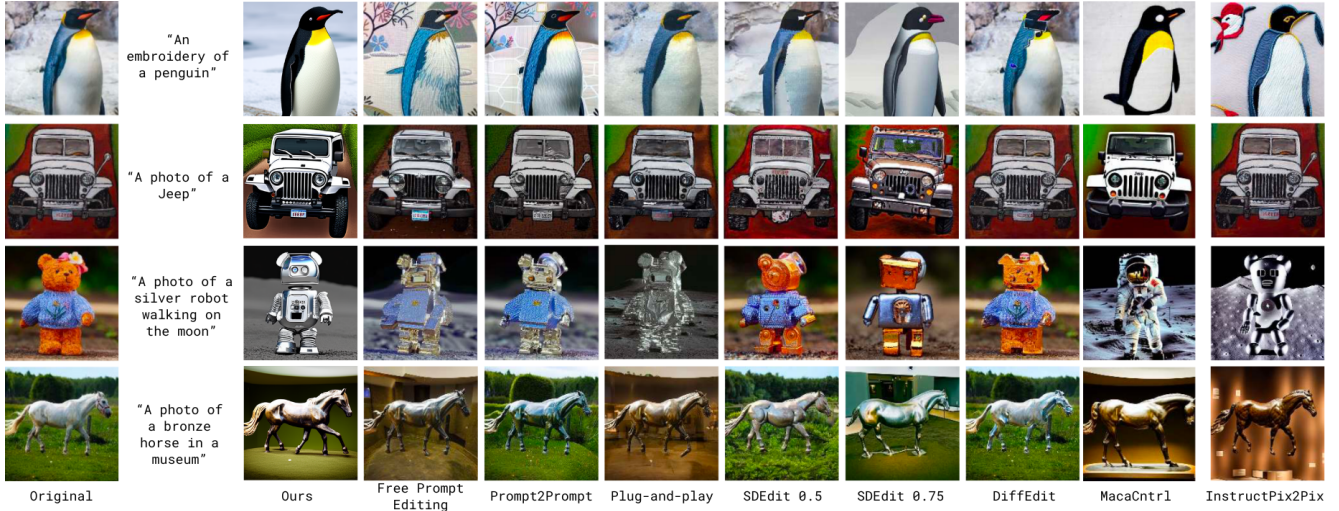


Figure 9. Qualitative comparison of different prompt-guided editing methods. We use as reference results proposed by [25] thus, we do not cherry-pick the results. From left to right: source image, target prompt, our result, Free Prompt Editing, P2P [13], PnP [46], SDEdit [27] with two noise levels, DiffEdit [10], Pix2pixzero [26], Shape-guided [30], MasaCtrl [6], and InstructPix2Pix [4] (a fine-tuning-based method).

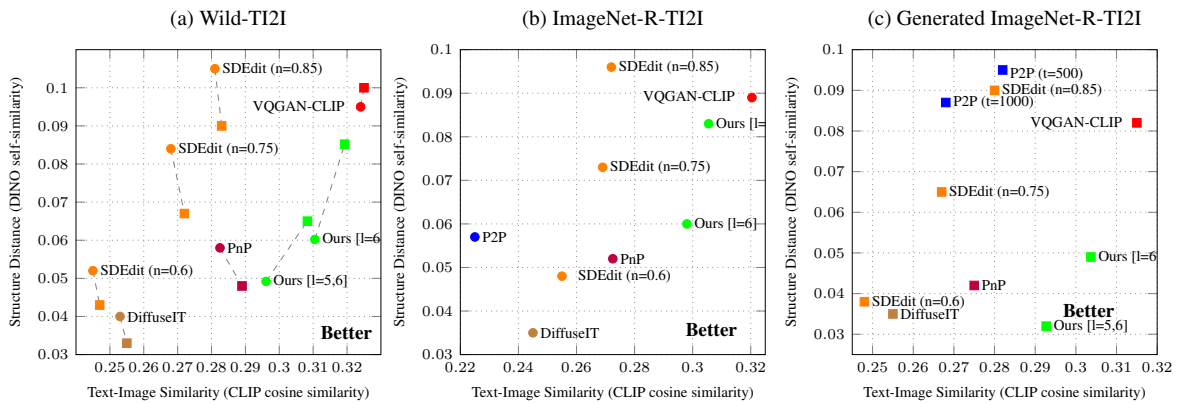


Figure 10. Quantitative evaluation. We measure CLIP cosine similarity (higher is better) and DINO-ViT self-similarity distance (lower is better) to quantify the fidelity to text and preservation of structure, respectively. We report these metrics on three benchmarks: (a) Wild-TI2I, (b) ImageNet-R-TI2I, and (c) Generated ImageNet-R-TI2I. [47]

painting” transformation, our model accurately replicates the brushstroke aesthetic and introduces a poppy field, typical of Impressionist painters, while maintaining the original shape and posture of the horse. Nonetheless, our method inherits certain biases from Stable Diffusion, resulting in inaccurate visual aesthetics for movements like Cubism, Futurism, and Dadaism despite successfully achieving stereotypical modifications.

Quantitative evaluation Our method, represented by **l=4,5** and **l=4** in Table 1, demonstrates strong alignment with text prompts while preserving content structure. On the CLIP Alignment metric, the **l=4** model achieves the highest score of 28.55, with **l=4,5** close behind at 26.27. These scores indicate that our model adheres effectively to prompt guid-

ance, achieving transformations that accurately reflect the target style. Regarding structural similarity, our **l=4,5** model attains an LPIPS score of 0.57, with **l=4** following at 0.67, demonstrating good content retention compared to most baseline models. These lower LPIPS values suggest that our approach maintains structural and perceptual fidelity to the original content, even under significant stylistic transformations. Competing methods, such as DDIM (0.74), DiffStyler (0.72), and ControlNet-Depth (0.78), display higher LPIPS scores, reflecting a greater degree of content distortion. Artist shows competing performance while obtaining inferior qualitative results.

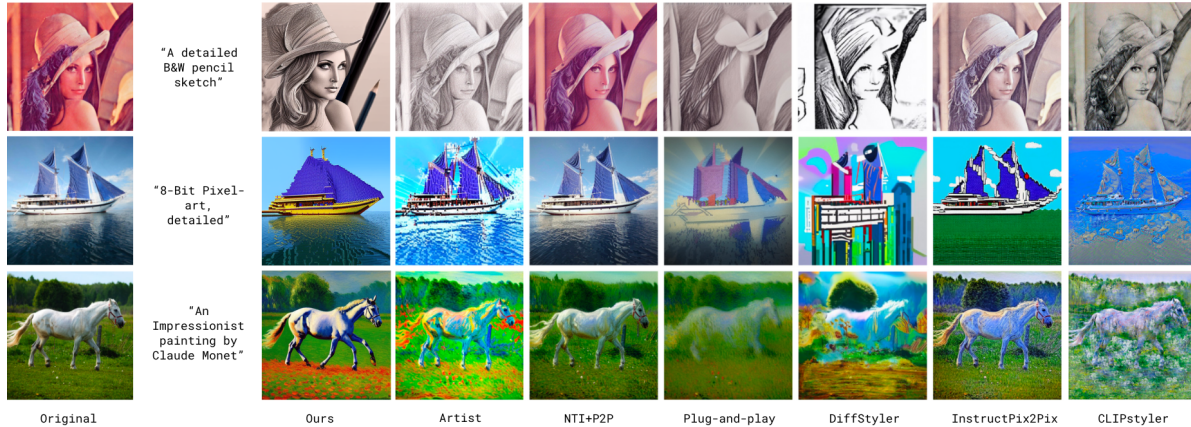


Figure 11. Qualitative evaluation against current style transfer methods. We use the reference results by [20], and we do not do any cherry-picking.

Table 1. Evaluation of Different Style Transfer Models on the Artist Dataset [20], measuring Content Preservation (LPIPS) and Stylization Prompt Alignment (CLIP Alignment).

Metric	Ours (l=4,5)	Ours (l=4)	Artist	DDIM	NTI-P2P	PnP	DiffStyler	InstructP2P	ControlNet-Canny	ControlNet-Depth	CLIPStyler
LPIPS ↓	0.57	0.67	0.62	0.74	0.67	0.67	0.72	0.47	0.72	0.78	0.51
CLIP Alignment ↑	26.27	28.55	28.33	28.38	25.87	26.4	26.82	23.59	26.4	27.05	26.14

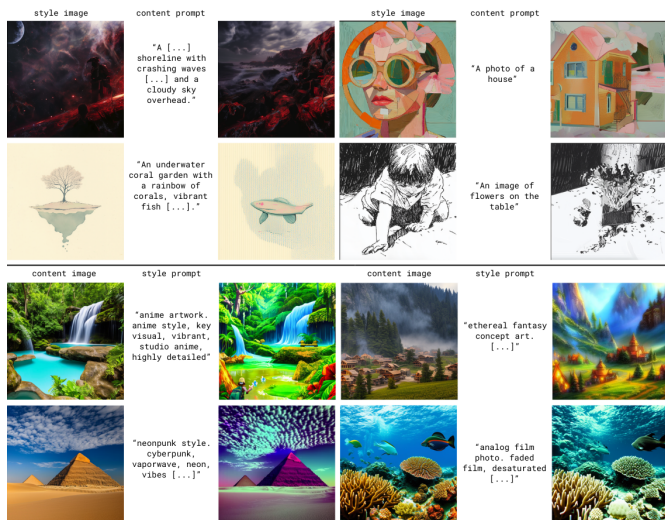


Figure 12. The AI Art online communities offer an incredible wealth of information on style transfer in blogs such as [Stable Diffusion Art](#) that could be leveraged to build applied benchmarks for style transfer. In this figure, we show two interesting applications of our method: the first consists of the transfer of closed-source styles (e.g., styles used in Midjourney) to Stable Diffusion outputs using single-image style transfer (on the left). The second leverages the style prompts (with respective negative prompts) released by [StabilityAI](#) to transfer the described styles to real images or selected generated images (on the right).

6. Conclusion

In conclusion, this paper explores the impact of U-Net skip connections in Stable Diffusion models, presenting a training-free, efficient approach—SkipInject—that enables high-quality text-guided image editing and style transfer. By systematically examining these skip connections, we address key questions about how spatial and stylistic information is encoded in the latent spaces of Stable Diffusion, the stages within the denoising process where they arise, and the structure of these spaces. Our findings reveal that specific skip connections are fundamental in controlling content and style, providing insight into how these components influence image generation.

The proposed method leverages the l=4 and l=5 skip connections to achieve precise style and content transfer, demonstrating state-of-the-art or on-par performance across established benchmarks. In addition, we introduce three modulation techniques for controlled editing intensity, offering flexible adjustments to meet diverse requirements.

Our approach currently relies on a single latent, limiting its application from scenarios that require dual-image style transfer. Future work will focus on extending SkipInject to support two-image inputs for broader applications.

References

- [1] Art walks in latent spaces, . 3
- [2] Inceptionism: Going Deeper into Neural Networks, . 3
- [3] Stable Diffusion 1 vs 2 - What you need to know, 2022. 1
- [4] Tim Brooks, Aleksander Holynski, and Alexei A Efros. InstructPix2pix: Learning to follow image editing instructions. In *Proceedings of the IEEE/CVF Conference on Computer Vision and Pattern Recognition*, pages 18392–18402, 2023. 7
- [5] Tim Brooks, Aleksander Holynski, and Alexei A. Efros. InstructPix2Pix: Learning To Follow Image Editing Instructions. pages 18392–18402, 2023. 3
- [6] Mingdeng Cao, Xintao Wang, Zhongang Qi, Ying Shan, Xiao-hu Qie, and Yinqiang Zheng. Masactrl: Tuning-free mutual self-attention control for consistent image synthesis and editing. In *Proceedings of the IEEE/CVF International Conference on Computer Vision*, pages 22560–22570, 2023. 7
- [7] Mathilde Caron, Hugo Touvron, Ishan Misra, Hervé Jégou, Julien Mairal, Piotr Bojanowski, and Armand Joulin. Emerging properties in self-supervised vision transformers. In *Proceedings of the IEEE/CVF international conference on computer vision*, pages 9650–9660, 2021. 6
- [8] Eva Cetinic. The Myth of Culturally Agnostic AI Models, 2022. arXiv:2211.15271 [cs]. 3
- [9] Paramanand Chandramouli. LDEdit: Towards Generalized Text Guided Image Manipulation via Latent Diffusion Models. 3
- [10] Guillaume Couairon, Jakob Verbeek, Holger Schwenk, and Matthieu Cord. Diffedit: Diffusion-based semantic image editing with mask guidance. *arXiv preprint arXiv:2210.11427*, 2022. 7
- [11] Rohit Gandikota, Joanna Materzynska, Tingrui Zhou, Antonio Torralba, and David Bau. Concept Sliders: LoRA Adaptors for Precise Control in Diffusion Models, 2023. arXiv:2311.12092 [cs]. 3
- [12] René Haas, Inbar Huberman-Spiegelglas, Rotem Mulyoff, Stella Graßhof, Sami S. Brandt, and Tomer Michaeli. Discovering Interpretable Directions in the Semantic Latent Space of Diffusion Models, 2023. 3
- [13] Amir Hertz, Ron Mokady, Jay Tenenbaum, Kfir Aberman, Yael Pritch, and Daniel Cohen-Or. Prompt-to-prompt image editing with cross attention control. *arXiv preprint arXiv:2208.01626*, 2022. 7
- [14] Amir Hertz, Ron Mokady, Jay Tenenbaum, Kfir Aberman, Yael Pritch, and Daniel Cohen-Or. Prompt-to-Prompt Image Editing with Cross Attention Control, 2022. arXiv:2208.01626 [cs]. 3
- [15] Irina Higgins, Loic Matthey, Arka Pal, Christopher Burgess, Xavier Glorot, Matthew Botvinick, Shakir Mohamed, and Alexander Lerchner. beta-VAE: Learning Basic Visual Concepts with a Constrained Variational Framework. 2016. 2
- [16] Jonathan Ho and Tim Salimans. Classifier-Free Diffusion Guidance. 2021. 5
- [17] Jonathan Ho, Ajay Jain, and Pieter Abbeel. Denoising Diffusion Probabilistic Models, 2020. arXiv:2006.11239 [cs, stat]. 2
- [18] Leonardo Impett and Fabian Offert. There Is a Digital Art History, 2023. arXiv:2308.07464 [cs]. 3
- [19] Jaeseok Jeong, Mingi Kwon, and Youngjung Uh. Training-Free Content Injection Using H-Space in Diffusion Models. pages 5151–5161, 2024. 3
- [20] Ruixiang Jiang and Changwen Chen. Artist: Aesthetically Controllable Text-Driven Stylization without Training, 2024. arXiv:2407.15842 [cs]. 3, 5, 6, 8
- [21] Tero Karras, Samuli Laine, and Timo Aila. A Style-Based Generator Architecture for Generative Adversarial Networks. pages 4401–4410, 2019. 2
- [22] Gwanghyun Kim, Taesung Kwon, and Jong Chul Ye. DiffusionCLIP: Text-Guided Diffusion Models for Robust Image Manipulation. In *2022 IEEE/CVF Conference on Computer Vision and Pattern Recognition (CVPR)*, pages 2416–2425, New Orleans, LA, USA, 2022. IEEE. 3
- [23] Diederik P. Kingma and Max Welling. Auto-Encoding Variational Bayes, 2022. arXiv:1312.6114 [cs, stat]. 2
- [24] Mingi Kwon, Jaeseok Jeong, and Youngjung Uh. Diffusion Models already have a Semantic Latent Space, 2023. arXiv:2210.10960 [cs]. 3, 5
- [25] Bingyan Liu, Chengyu Wang, Tingfeng Cao, Kui Jia, and Jun Huang. Towards Understanding Cross and Self-Attention in Stable Diffusion for Text-Guided Image Editing, 2024. arXiv:2403.03431 version: 1. 3, 5, 7
- [26] Matthew Martinez, Steven Hernandez, Joseph Davis, William Rodriguez, and Paul Lopez. Introducing pix2pix-zero: Efficient and effective zero-shot image-to-image translation with diffusion models. 7
- [27] Chenlin Meng, Yutong He, Yang Song, Jiaming Song, Jiajun Wu, Jun-Yan Zhu, and Stefano Ermon. Sedit: Guided image synthesis and editing with stochastic differential equations. *arXiv preprint arXiv:2108.01073*, 2021. 7
- [28] Chong Mou, Xintao Wang, Liangbin Xie, Yanze Wu, Jian Zhang, Zhongang Qi, Ying Shan, and Xiao-hu Qie. T2I-Adapter: Learning Adapters to Dig out More Controllable Ability for Text-to-Image Diffusion Models, 2023. arXiv:2302.08453. 3
- [29] Rishabh Parihar, Sachidanand VS, Sabariswaran Mani, Tejan Karmali, and R. Venkatesh Babu. PreciseControl: Enhancing Text-To-Image Diffusion Models with Fine-Grained Attribute Control, 2024. arXiv:2408.05083 [cs]. 3
- [30] Dong Huk Park, Grace Luo, Clayton Toste, Samaneh Azadi, Xihui Liu, Maka Karalashvili, Anna Rohrbach, and Trevor Darrell. Shape-guided diffusion with inside-outside attention. In *Proceedings of the IEEE/CVF Winter Conference on Applications of Computer Vision*, pages 4198–4207, 2024. 7
- [31] William Peebles and Saining Xie. Scalable Diffusion Models with Transformers, 2023. arXiv:2212.09748 [cs]. 2
- [32] Dustin Podell, Zion English, Kyle Lacey, Andreas Blattmann, Tim Dockhorn, Jonas Müller, Joe Penna, and Robin Rombach. SDXL: Improving Latent Diffusion Models for High-Resolution Image Synthesis, 2023. arXiv:2307.01952. 1
- [33] Alec Radford, Jong Wook Kim, Chris Hallacy, Aditya Ramesh, Gabriel Goh, Sandhini Agarwal, Girish Sastry, Amanda Askell, Pamela Mishkin, Jack Clark, Gretchen

- Krueger, and Ilya Sutskever. Learning Transferable Visual Models From Natural Language Supervision, 2021. arXiv:2103.00020. 1
- [34] Alec Radford, Jong Wook Kim, Chris Hallacy, Aditya Ramesh, Gabriel Goh, Sandhini Agarwal, Girish Sastry, Amanda Askell, Pamela Mishkin, Jack Clark, et al. Learning transferable visual models from natural language supervision. In *International conference on machine learning*, pages 8748–8763. PMLR, 2021. 6
- [35] Aditya Ramesh, Prafulla Dhariwal, Alex Nichol, Casey Chu, and Mark Chen. Hierarchical Text-Conditional Image Generation with CLIP Latents, 2022. arXiv:2204.06125. 2
- [36] Nuria Rodríguez-Ortega. Techno-Concepts for the Cultural Field: n-Dimensional Space and Its Conceptual Constellation. *Multimodal Technologies and Interaction*, 6(11):96, 2022. 3
- [37] Robin Rombach, Andreas Blattmann, Dominik Lorenz, Patrick Esser, and Björn Ommer. High-Resolution Image Synthesis With Latent Diffusion Models. pages 10684–10695, 2022. 1, 4
- [38] Olaf Ronneberger, Philipp Fischer, and Thomas Brox. U-Net: Convolutional Networks for Biomedical Image Segmentation, 2015. arXiv:1505.04597 [cs]. 2, 4
- [39] Nataniel Ruiz, Yuanzhen Li, Varun Jampani, Yael Pritch, Michael Rubinstein, and Kfir Aberman. DreamBooth: Fine Tuning Text-to-Image Diffusion Models for Subject-Driven Generation. pages 22500–22510, 2023. 3
- [40] Christoph Schuhmann, Romain Beaumont, Richard Vencu, Cade Gordon, Ross Wightman, Mehdi Cherti, Theo Coombes, Aarush Katta, Clayton Mullis, Mitchell Wortsman, Patrick Schramowski, Srivatsa Kundurthy, Katherine Crowson, Ludwig Schmidt, Robert Kaczmarczyk, and Jenia Jitsev. LAION-5B: An open large-scale dataset for training next generation image-text models, 2022. arXiv:2210.08402. 1
- [41] Nick Seaver. Everything lies in a space: cultural data and spatial reality. *Journal of the Royal Anthropological Institute*, 27(S1):43–61, 2021. eprint: <https://onlinelibrary.wiley.com/doi/pdf/10.1111/1467-9655.13479>. 3
- [42] Yujun Shen, Ceyuan Yang, Xiaoou Tang, and Bolei Zhou. InterFaceGAN: Interpreting the Disentangled Face Representation Learned by GANs. *IEEE Transactions on Pattern Analysis and Machine Intelligence*, 44(4):2004–2018, 2022. Conference Name: IEEE Transactions on Pattern Analysis and Machine Intelligence. 2
- [43] Jascha Sohl-Dickstein, Eric A. Weiss, Niru Maheswaranathan, and Surya Ganguli. Deep Unsupervised Learning using Nonequilibrium Thermodynamics, 2015. arXiv:1503.03585. 2
- [44] Jiaming Song, Chenlin Meng, and Stefano Ermon. Denoising Diffusion Implicit Models, 2022. arXiv:2010.02502 [cs]. 3
- [45] Nick Stracke, Stefan Andreas Baumann, Joshua M. Susskind, Miguel Angel Bautista, and Björn Ommer. CTRLorALter: Conditional LoRAadapter for Efficient 0-Shot Control & Altering of T2I Models, 2024. arXiv:2405.07913 [cs]. 3
- [46] Narek Tumanyan, Michal Geyer, Shai Bagon, and Tali Dekel. Plug-and-play diffusion features for text-driven image-to-image translation. In *Proceedings of the IEEE/CVF Conference on Computer Vision and Pattern Recognition*, pages 1921–1930, 2023. 7
- [47] Narek Tumanyan, Michal Geyer, Shai Bagon, and Tali Dekel. Plug-and-Play Diffusion Features for Text-Driven Image-to-Image Translation. pages 1921–1930, 2023. 3, 5, 6, 7
- [48] Ted Underwood. Mapping the Latent Spaces of Culture. 2021. 3
- [49] Ted Underwood and Richard Jean So. Can We Map Culture? *Journal of Cultural Analytics*, 6(3), 2021. 3
- [50] Max Weisbuch, Sarah A. Lamer, Evelyne Treinen, and Kristin Pauker. Cultural snapshots: Theory and method. *Social and Personality Psychology Compass*, 11(9):e12334, 2017. eprint: <https://onlinelibrary.wiley.com/doi/pdf/10.1111/spc3.12334>. 3
- [51] Lvmin Zhang, Anyi Rao, and Maneesh Agrawala. Adding Conditional Control to Text-to-Image Diffusion Models, 2023. arXiv:2302.05543 [cs]. 3
- [52] Richard Zhang, Phillip Isola, Alexei A Efros, Eli Shechtman, and Oliver Wang. The unreasonable effectiveness of deep features as a perceptual metric. In *Proceedings of the IEEE conference on computer vision and pattern recognition*, pages 586–595, 2018. 6
- [53] Ye Zhu, Yu Wu, Zhiwei Deng, Olga Russakovsky, and Yan Yan. Boundary Guided Learning-Free Semantic Control with Diffusion Models, 2023. arXiv:2302.08357 [cs]. 3

Training-Free Style and Content Transfer by Leveraging U-Net Skip Connections in Stable Diffusion 2.*

Supplementary Material

In this Supplementary Material, we present the following sections to support the findings of the main paper:

- **effect of different versions of Stable Diffusion** where we show the impact of SkipInject on Stable Diffusion 1.4, 1.5, 2, 2.1, Turbo, and XL and find that 1.4-1.5 and XL share a similar representation split that differs from all 2.* versions treated in the paper.
- **ablation studies on the hyperparameters** where we show our model’s qualitative and quantitative results on different combinations of the hyperparameters both for style transfer and text-guided image editing.
- **examples on Turbo** where we show examples generated using SkipInject on Turbo, showing extremely promising results on one-step inference.

7. Effect of different versions of Stable Diffusion

The main paper focuses on Stable Diffusion v2.0. In this Supplementary Material section, we investigate whether the phenomenon identified on Stable Diffusion v2.0 extends to other versions of UNet-based Stable Diffusions and whether the previously observed importance of the h -space, presented in the Introduction, can be found in other versions. To understand whether the models form different representations, we carry out the same experiment on different versions of Stable Diffusion. We find that Stable Diffusion 2 and 2.1 behave similarly, as well as the Turbo version of 2.1, while Stable Diffusion 1.4, 1.5, and XL show a more profound impact of the h -space, shown in Fig. 13.

In terms of architecture, the significant difference between Stable Diffusion v1.* and Stable Diffusion v2.* lies in the text embedding used for conditioning: the first versions use OpenAI’s CLIP [33]. In contrast, the second versions use OpenCLIP, trained on the publicly available LAION 2B dataset [40]. Furthermore, Stable Diffusion v2.* uses a longer context length than v1.*, supporting a larger output size (from 512 to 768). The rest of the architecture remains unchanged. Stable Diffusion 2.*, despite producing higher resolution outputs, has seen a lower adoption, likely due to its incompatibility with the prompt engineered on versions 1.*[3].

Our analysis shows that the earlier versions put a much higher weight on the h -space, indicating an evolution in the representations learned by these models. Given that most of the architecture remains unchanged, we can hypothesize that the CLIP embeddings cause the difference.

Stable Diffusion XL [32] is the last UNet-based model

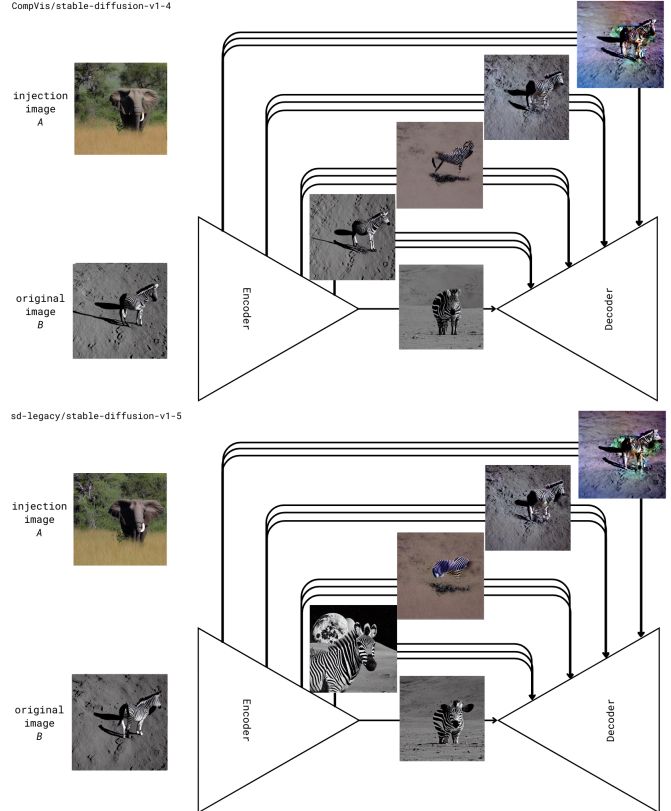


Figure 13. Visualization of SkipInject effect on v1.4 and v1.5. As visible in the figure, the effect of the second group of skip connections is now split between the h -space, carrying the content of the foreground, and the second group of skips, determining the content of the background without structure.

released by StabilityAI. This model is about 4x larger than the previous Stable Diffusions and comprises base and refiner models. This section considers the base model responsible for generating the overall image. As visible in Fig. 15, this model only features three downsampling blocks, with seldom cross-attentions in the first blocks and a concentration of the attention modules before the bottleneck. This model accepts two conditioning embeddings, one from OpenAI’s CLIP, as in v1.*, and one from OpenCLIP, a larger version than the one used in v2.*. Because of this dual prompt, Stable Diffusion XL allows broader expressivity and the desired compatibility with v1.*.

In Fig. 15, we observe that, interestingly, Stable Diffusion XL behaves very similarly to v1.*. While the spec-

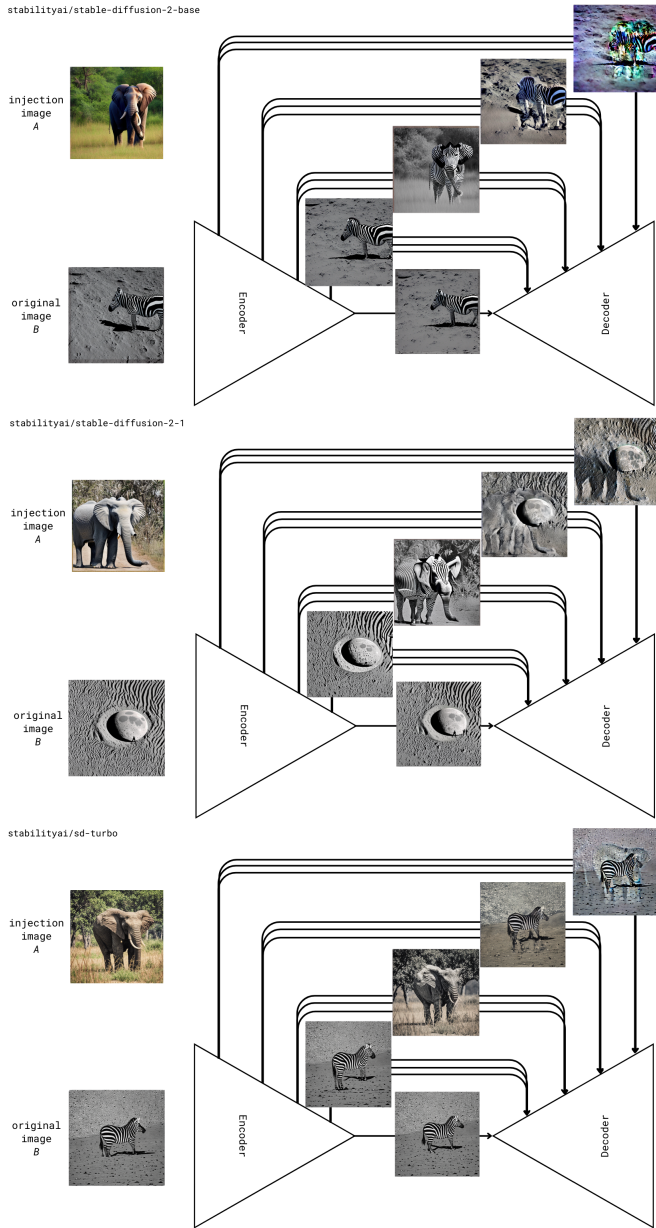


Figure 14. Visualization of SkipInject effect on v2, v2.1, v2.1 Turbo. As visible in the figure, these three models have very similar effects. The content representation passes almost exclusively through the second group of skip connections, even in distilled Turbo versions.

ulation on the importance of the CLIP version still seems plausible, this phenomenon requires much deeper investigation, possibly underscoring studies on Diffusion models as representation learners.

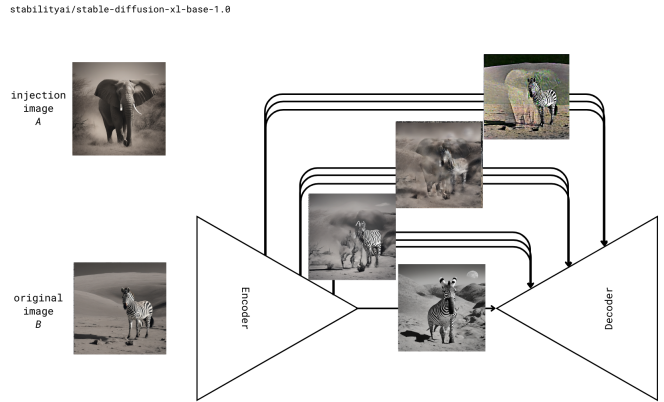


Figure 15. Visualization of SkipInject effect on XL. As visible in the figure, the effect of the second group of skip connections is, as for v1.*, split between the h -space, where the orientation and structure of the foreground are determined, and the second group of skips, determining the content of the background, without structure.

8. Ablation studies on the hyperparameters

In this section, we test different configurations of the hyperparameters to ablate on our findings reported in the section Analyses. In that section, we recommend an ending timestep ≥ 350 (indicated in the field **Injection t.**) to show the background specified by the modification and an interplay of the alternation (here referred to as **Altern.**, indicating every how often the injected embedding is substituted in depth with the original one) and guidance on the injected embedding (here referred to as **Switch g.**) for an improved tradeoff between the ability to follow the semantic editing and the maintenance of the structure.

In the Tab. 2 and Tab. 3, we show, respectively, the prompt-to-image results on ImageNet and Wild. While in Tab. 4 and Tab. 5, we present the results on image-to-image. The results are obtained with 50 inference steps (and inversion steps), UniPCMultistepScheduler, output size (512,512,) and classifier-free guidance 7.5.

Generally, we observe that an injection across all timesteps yields the most structural fidelity. Using switch guidance greater than one further decreases the DINO self-similarity and LPIPS. The highest prompt coherence is achieved by an interplay of switch guidance and alternation, with optimal results obtained on skips $l=4,5$.

9. Examples on Turbo

We show example results on Stable Diffusion Turbo.

Skip	Injection t.	Switch g.	Altern.	CLIP	DINO	LPIPS
l=4	(0, 1000)	None	None	0.289	0.033	0.421
l=4,5	(0, 1000)	None	None	0.278	0.018	0.291
l=4	(400, 900)	None	None	0.301	0.045	0.497
l=4,5	(400, 900)	None	None	0.291	0.029	0.375
l=4	(400, 900)	0.75	None	0.306	0.060	0.560
l=4,5	(400, 900)	0.75	None	0.296	0.041	0.456
l=4	(400, 900)	0.75	10	0.308	0.065	0.581
l=4,5	(400, 900)	0.75	10	<i>0.299</i>	<i>0.048</i>	<i>0.497</i>
l=4	(400, 900)	0.75	20	0.308	0.062	0.569
l=4,5	(400, 900)	0.75	20	0.297	0.045	0.476
l=4	(400, 900)	1.5	None	0.297	0.039	0.460
l=4,5	(400, 900)	1.5	None	0.284	0.024	0.341

Table 2. Ablation results on `imnetr-fake-ti2i` dataset. The best scores are indicated with bold, while the one considered the best compromise in italics. The metric named CLIP indicates CLIP score (higher better), DINO is the DINO self-similarity (lower better, as for LPIPS). The lowest DINO and LPIPS are achieved by the standard model across all timesteps using skips $l=4,5$, while the interplay of switch guidance and alternation achieves the highest CLIP scores. We believe $l=4,5$, with both guidance and alternation, achieves the best tradeoff on this dataset.

Skip	Injection t.	Switch g.	Altern.	CLIP	DINO	LPIPS
l=4	(0, 1000)	None	None	0.303	0.063	0.523
l=4,5	(0, 1000)	None	None	0.268	0.036	0.341
l=4	(400, 900)	None	None	0.308	0.080	0.564
l=4,5	(400, 900)	None	None	0.294	0.062	0.441
l=4	(400, 900)	0.75	None	0.313	0.093	0.593
l=4,5	(400, 900)	0.75	None	0.302	0.070	0.495
l=4	(400, 900)	0.75	10	0.316	0.101	0.621
l=4,5	(400, 900)	0.75	10	0.307	0.080	0.532
l=4	(400, 900)	0.75	20	0.315	0.097	0.610
l=4,5	(400, 900)	0.75	20	<i>0.303</i>	<i>0.073</i>	<i>0.510</i>
l=4	(400, 900)	1.5	None	0.305	0.077	0.542
l=4,5	(400, 900)	1.5	None	0.286	0.056	0.413

Table 3. Ablation results on `wild-ti2i-fake` dataset. Similarly to Tab. 2, the lowest DINO and LPIPS are achieved by the standard model across all timesteps using skips $l=4,5$. In contrast, the interplay of switch guidance and alternation achieves the highest CLIP scores. Differently from Tab. 2, the best tradeoff is achieved with an alternation every 20 instead of 10. A higher alternation indicates lower modulation as to how often the embedding of the original image is injected into the injection embedding in depth.

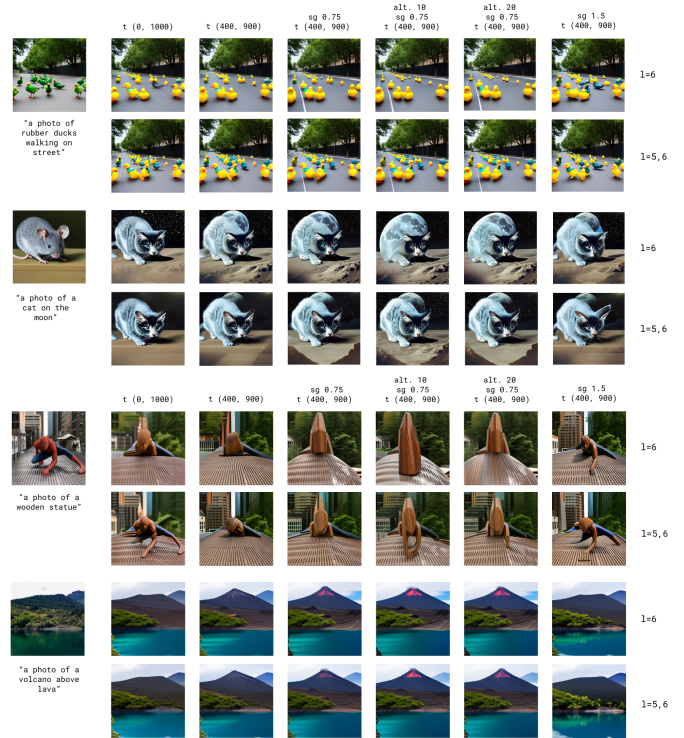


Figure 16. Example results of text-guided image editing both on generated images (top) and inverted images (bottom) on different configurations of hyperparameters. We observe that, across most images, the base configuration already achieves reasonable results. When the background is specified (second image from the top), fewer injection timesteps contribute to forming the correct background. On the other side, the switch guidance and alternation strengthen the importance of the editing prompt, becoming particularly visible on the fourth image, whether the lava appears only when introducing switch guidance and the corresponding smoke with alternation.

Skip	Injection t.	Switch g.	Altern.	CLIP	DINO	LPIPS
l=4	(0, 1000)	None	None	0.288	0.059	0.524
l=4,5	(0, 1000)	None	None	0.275	0.047	0.494
l=4	(400, 900)	None	None	0.295	0.066	0.540
l=4,5	(400, 900)	None	None	0.287	0.052	0.505
l=4	(400, 900)	0.75	None	0.302	0.078	0.567
l=4,5	(400, 900)	0.75	None	<i>0.300</i>	<i>0.067</i>	<i>0.540</i>
l=4	(400, 900)	0.75	10	0.306	0.084	0.577
l=4,5	(400, 900)	0.75	10	0.301	0.073	0.556
l=4	(400, 900)	0.75	20	0.303	0.081	0.573
l=4,5	(400, 900)	0.75	20	0.300	0.069	0.546
l=4	(400, 900)	1.5	None	0.290	0.056	0.515
l=4,5	(400, 900)	1.5	None	0.278	0.046	0.483

Table 4. Ablation results on `imnetr-ti2i-real` dataset. On this dataset, despite using fewer timesteps than the base configuration, the lowest DINO and LPIPS are achieved by switch guidance 1.5 using skips $l=4,5$. Differently from Tab. 2 and Tab. 3, the best tradeoff is achieved without any alternation on switch guidance 0.75.

Skip	Injection t.	Switch g.	Altern.	CLIP	DINO	LPIPS
l=4	(0, 1000)	None	None	0.290	0.046	0.499
l=4,5	(0, 1000)	None	None	0.272	0.038	0.457
l=4	(400, 900)	None	None	0.298	0.054	0.513
l=4,5	(400, 900)	None	None	0.282	0.044	0.468
l=4	(400, 900)	0.75	None	0.305	0.064	0.540
l=4,5	(400, 900)	0.75	None	0.296	0.055	0.502
l=4	(400, 900)	0.75	10	0.307	0.068	0.549
l=4,5	(400, 900)	0.75	10	<i>0.302</i>	<i>0.059</i>	<i>0.515</i>
l=4	(400, 900)	0.75	20	0.305	0.066	0.544
l=4,5	(400, 900)	0.75	20	0.300	0.057	0.508
l=4	(400, 900)	1.5	None	0.289	0.049	0.486
l=4,5	(400, 900)	1.5	None	0.271	0.040	0.447

Table 5. Ablation results on `wild-ti2i-real` dataset. On this dataset, the lowest DINO is achieved by the base configuration while the lowest LPIPS are achieved by switch guidance 1.5 using skips l=4,5. Similarly to Tab. 2, the best tradeoff is obtained with alternation 10 and switch guidance 0.75.



Figure 17. Example results of style transfer on different configurations of hyperparameters. We observe that the standard configuration yields the most structurally sound results, but fails to transfer the style to the background. Using fewer timesteps and guidance or alternation increases the effect, also adjusting the subjects to be more coherent within that style.

Skip	Injection t.	Switch g.	Altern.	CLIP	DINO	LPIPS
l=4	(0, 1000)	None	None	0.217	0.036	0.481
l=4,5	(0, 1000)	None	None	0.186	0.025	0.398
l=4	(400, 900)	0.75	None	0.263	0.054	0.580
l=4,5	(400, 900)	0.75	None	0.236	0.037	0.483
l=4	(400, 800)	0.75	None	0.270	0.060	0.608
l=4,5	(400, 800)	0.75	None	0.248	0.041	0.515
l=4	(400, 900)	0.65	None	0.271	0.062	0.613
l=4,5	(400, 900)	0.65	None	0.252	0.044	0.528
l=4	(400, 900)	0.65	15	0.276	0.067	0.631
l=4,5	(400, 900)	0.65	15	<i>0.260</i>	<i>0.050</i>	<i>0.559</i>

Table 6. Ablation results on `artist` dataset. On this dataset, the lowest DINO and LPIPS are achieved by the base configuration using skips l=4,5, while the highest CLIP with switch guidance 0.65 and alternation 15 on skip 4. The l=4,5 (sg 0.65, alt 15) achieves the optimal configuration, lower in switch guidance and higher in alternation than text-based editing.

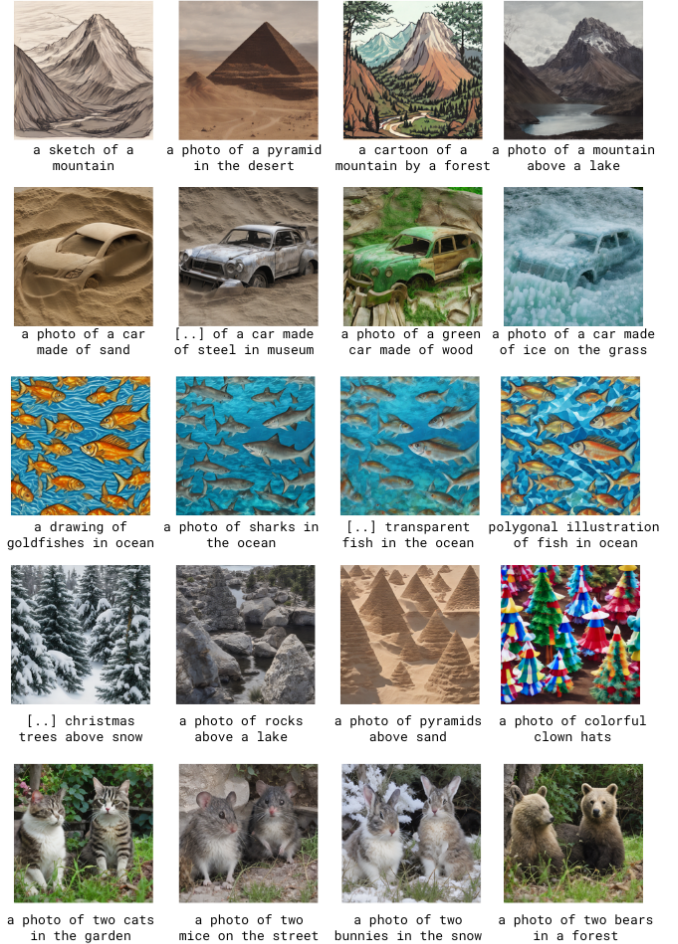


Figure 18. Example results of text-based image editing using Stable Diffusion Turbo with 1 step inference on `wild-ti2i-fake`. The modifications obtained are coherent and cohesive, obtaining radical changes and maintaining the original structure. Compared to multi-step inference, the control over the background is more limited.